Proceedings: The 16th International Seminar On Double Layer Capacitors,
Deerfield Beach, FL., U.S.A., December 4-6, 2006.

Capacitance Determination and Abusive Aging Studies of Supercapacitors Based on Acetonitrile and Ionic Liquids

P. KURZWEIL[1], M. CHWISTEK

[1)] University of Applied Sciences, Kaiser-Wilhelm-Ring 23, D-92224 Amberg, Germany

R. GALLAY[2]

[2)] Maxwell Technologies, CH-1728 Rossens, Switzerland

Abstract. a) We studied some safety aspects related to the operation of supercapacitors based on acetonitrile, especially the decomposition products of electrodes and electrolytes during abusive testing at voltages of up to 6 V and temperatures up to 90 °C. Ethylene, volatile amines, intermediate amides, carboxylate anions of organic acids, fluorinated and heterocyclic compounds are formed in the electrolyte. Nevertheless, life-times of several months can be estimated even on destructive operating conditions (90°C). Inflammation or explosions were not observed in any case of abusive testing. – b) Double-layer capacitors of different manufacturers were characterized by *ac* impedance spectroscopy, cyclic voltammetry, and transient methods. We were able to gather scaling factors for the conversion of *ac* series impedance capacitances at 1 Hz into values corresponding to *dc* transient techniques: roughly a factor of 1.5 (acetronitrile) to 5 (propylencarbonate) for commercial capacitors in the 100 F range. – c) State-of-the-art ionic liquids were characterized in supercapacitors. Without laborious and costly purfication steps, however, the "best" ionic liquids in the test provided a 35% smaller potential window and a tenfold lower conductivity than the acetonitrile system. Hence, acetonitrile cannot easily be replaced by different low-cost electrolyes in near future.

1 Aging behaviour of supercapacitors on abusive conditions

1.1 Accelerated aging tests

Figure 1 shows that capacitance falls dramatically if supercapacitors are stored at an ambient temperature of 90°C and an applied voltage of 2.3 V. Nevertheless, supercapacitors can be operated on these rigorous conditions at least temporarily. All capacitors fail due to the increasing internal resistance. The nearby exponential decline of capacitance follows the ARRHENIUS equation. With this, lifetime of a 50 F Japanese supercapacitor *B* can be estimated by roughly 4.6 months (at 2.5 V) to 7.7 months (2,3 V) and 12.5 month (2.1 V) at 90°C, until the internal resistance quadruples to a value of about 600 mΩ. Lowering operating voltage by 0.4 V stretches lifetime by a factor of about three (2.7).

Double-layer capacitors suffer a rise of the equivalent series resistance by a factor of 0.5 to 5 during the first 1000 hours of operation at rated voltage (2.5 V) and ambient temperatures between 70 and 90 °C (see **Figure 2**). The decrease of capacitance by about 10% is far less affected by heat [1].

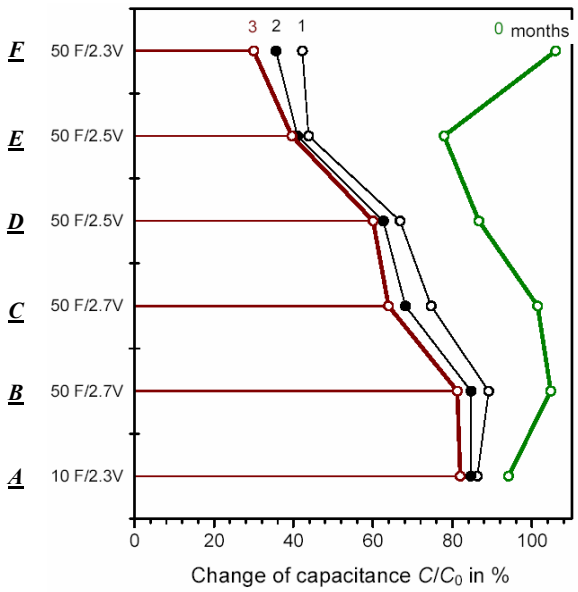

Fig. 1: Ratio of measured capacitance C and rated capacitance C_0 (printed on the case) after storage at 90 °C and 2.3 V. *A* to *F*: different manufacturers from Asia, Europe and America.

1.2 Decomposition products after abuse testing

With respect to the scarce knowledge in literature [4], we were able to gather the first detailed insights into the thermal and electrochemical decomposition mechanisms of tetraethylammonium-tetrafluoroborate in acetonitrile by help of GC-MS, UV und IR spectroscopy, thermogravimetric analysis, and X-ray diffraction [2,3]. Our results in short:

1. Unwanted traces of water in the electrolyte and carbon electrodes cause the hydrolysis of acetonitrile, whereby *acetamide* and *organic acids* are formed (below 4 V). Above a cell voltage of 6 V derivates of fluoroacetic acid are found.
2. In the liquid phase *heterocyclic compounds* are formed such as pyrazines. Water is generated by condensation of amino-carbonyl compounds.
3. The alkylammonium cation is destroyed by the elimination of *ethylene*. The trialkylamine by-product can be oxidised further.
4. Tetrafluoroborate is a source of fluoride, *hydrogenfluoride* and boric acid (metaborate).
5. Leaky capacitors lose a brownish crystalline mass, which consists of residual supporting electrolyte and active carbon, organic acids, acetamide, and polyoles. We were able to reproduce the deposits by electrolysis of a saturated solution of $[(CH_3CH_2)_4N]BF_4$ in acetonitrile.
6. The active carbon electrodes (Figure 2) lose cyclic siloxanes and *aromatic contaminations* even at room temperature, and are destroyed mainly by the anodic reaction. The electrodes catalyze the thermal decompositon of the $TEABF_4$ electrolyte.
7. The oxide layer on the etched aluminium support material under the active carbon layer is destroyed by fluorination. This process acts as a source of oxygen.
8. *Hydrogen* is generated by electrolysis of water and by the fluorination of carboxylic acids.

1.3 Salt residues in burst capacitors

The X-ray diffractogram (**Figure 3**) of the brownish salt residues at burst ultracapacitors, which failed after a long time of operation at high voltages, gives hints at acetamide, aromatic and unsaturated organic acids, fluoroacetic acid derivates and macromolecular products. The unexpected variety of compounds in this crystalline mass is partly due to several weeks of storing in ambient air. The XRD results, indicating the presence of amides, were verified by IR spectroscopy (Figure 6) and thermal analysis (Figure 7).

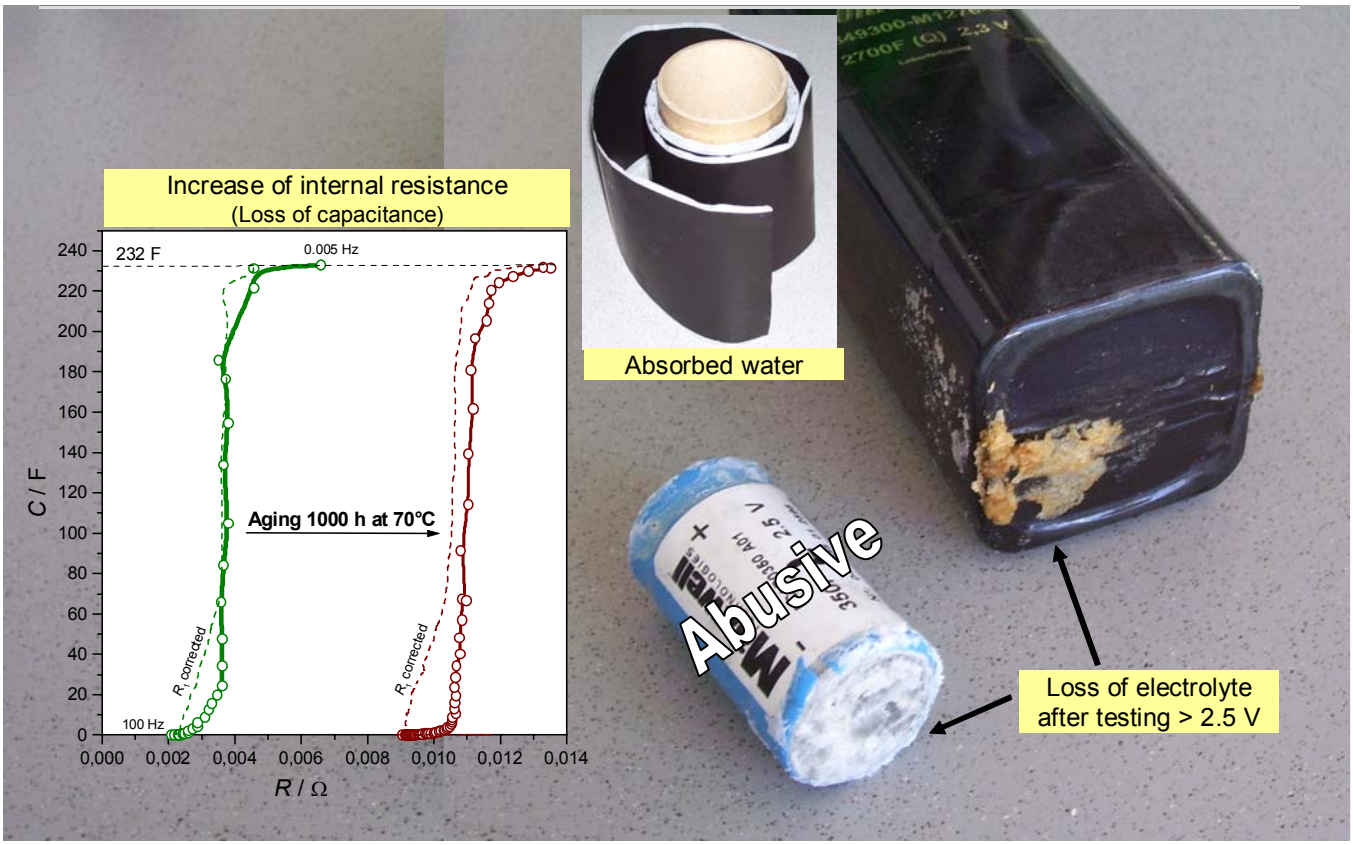

Fig. 2: *Left:* Increase of resistance after thermal aging. *Right:* Salt deposits on burst supercapacitors after several thousand hours of operation including abusive high temperatures (up to 90°C) and temporary voltag peaks (up to 3...5 V). *Above:* Active carbon/aluminium electrode.

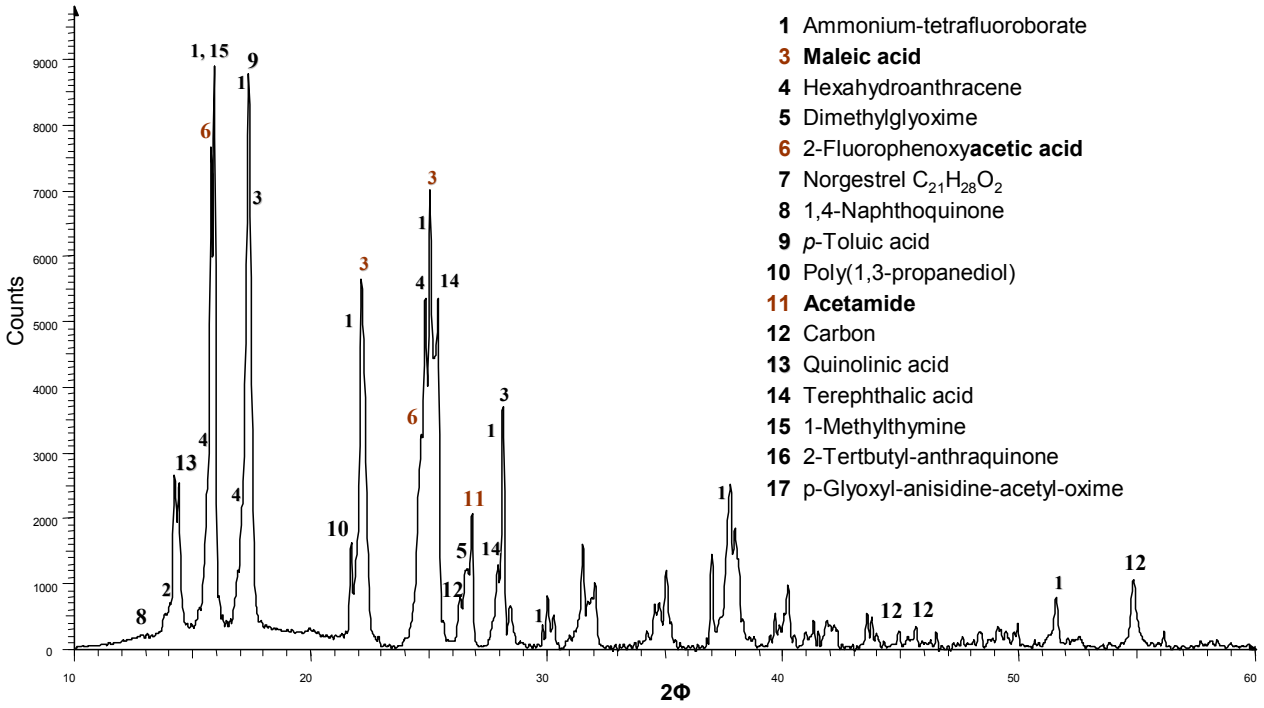

Fig. 3: X-ray diffractogram (XRD) of the salt residue on the ultracapacitor in Figure 2. The products, mainly organic amides and acids, are not considered as harmful. Toxic cyanides were not found.

Accelerated aging by electrolysis. We reproduced a similar crystalline mass by electrolysis of the electrolyte at 4 V (see **Figure 4**). The formation of fluorocarboxylic acids requires a cell voltage of about 6 V. Acid gases escape. In the residual electrolyte we could identify fluoride and borates by precipitation with calcium and silver ions. Obviously *hydrogen-fluoride* is formed. Heating the crystals in a glass vial, the characteristic oily gas bubbles creep up the etched glass walls. At a decomposition voltage of 4 V, considerable gas formation was not observed.

Pure acetonitrile, and the electrolyte solution do not absorb **UV/VIS** light below 800 nm (**Figure 5**). After 10 hours of electrolysis in a gas-tight vessel, flooded with nitrogen, however, marked absorption peaks arise, which are similar to those of the crystals on the burst ultracapacitor, dissolved in acetonitrile. The strong peak at 220 nm is also found in acetamide, bands of organic acids occur at somewhat lower wavelength. The absorption peak at 260 nm is typical of the chromophoric group C=N, and the $\pi \rightarrow \pi^*$ transition in *aromatic* double bonds [5].

The **IR** spectra of the anode and cathode films in **Figure 6** give clear hints at the formation of intermediate amides and *carboxylate ions*. Tiny shoulders at ~1700, 1636 and 1435 cm^{-1} indicate unsaturated organic acids, although they are covered by stronger bands. A small portion of acetonitrile seems to dimerisate and to form maleic acid by hydrolysis. The quite similar cathodic conversion of

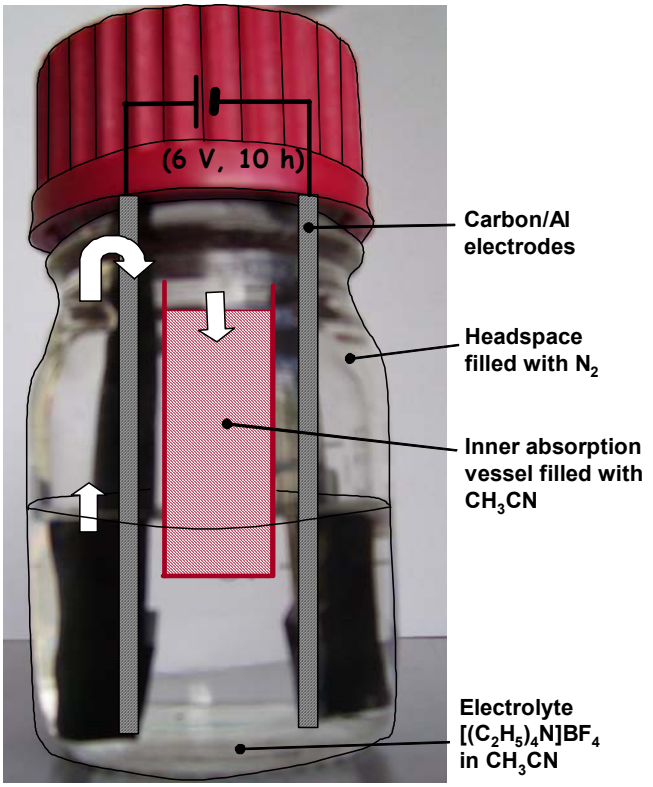

Fig. 4: Model experiment in a reaction bottle containing two active carbon electrodes in acetonitrile/$TEABF_4$. The screw-cap contains a polymer septum to allow headspace GC-MS analysis.

acrylonitrile to adiponitrile is well-known in organic electrosynthesis. The peaks at 1340 and 1616 cm^{-1}, typical of fluoroacetate, disappear after several weeks of storing at ambient air.

Acetamide and *organic acid* derivates are generated by hydrolysis of acetonitrile, a well-known reaction in organic chemistry. Derivates of *fluoroacetic acid* stem from a different reaction route by hydrohalogenation, in which aromatic hydrocarbons in the carbon electrodes play a role (**Figure 6b**). This is consistent to the fact, that the electrochemical fluorination of carboxylic acids in hydrogenfluoride by the SIMONS' process requires cell voltages of 5 to 8 V.

$$C_nH_{2n+1}COOH + (2n+1)HF \rightarrow C_nF_{n+1}COOH + (2n+1)H_2$$

With respect to the polymer-like characteristics of the deposits, we assume the formation of *polyamides* during electrolysis. IR spectra, not shown here, might indicate polyamides by the shoulder at 3050 cm^{-1}, and the IR bands at 1650 cm^{-1} and 1560 cm^{-1}, related to NH-vibrations (superimposed by water).

The *thermogravimetric curves* of the electrolytic deposits in **Figure 7** exhibit a step at 225°C which can be reproduced by the decomposition of acetamide. The main step at 495°C is due to the decomposition of mainly the alkylammonium ion followed by the more stable tetrafluoroborate. Dry active carbon electrodes show a linear decay up to 450 °C due to desorbing water, followed by two steps at 620°C and 840°C. The transition at 620°C is also found in the anodic residue of the electrolysis experiment.

1.4 Reactions in the liquid electrolyte

In the headspace GC-MS analysis of the electrolysis experiment we found the masses 41 (acetonitrile), 29 (ethyl), 20 (HF) and hints at complicated products.

The brown deposits on the electrodes and on the burst ultracapacitor, existing after electrolysis only, led us to the analogy of the MAILLARD reaction shown in **Figure 8**. We found *pyrazine* structures and oxidation products of *triethylamine* in the liquid and gaseous phase of our closed model reactor (Figure 4). It is noteworthy that the deposits smell of 2-acetyl-pyrazine, similar to the taste of popcorn. Certainly, further investigations must be conducted to clarify the nature of the *heterocyclic compounds* and fluorinated aromatic hydrocarbons, which are generated by the electrolysis of acetonitrile/$N(CH_2CH_3)_4BF_4$ at carbon electrodes at cell voltages above 4 – 6 V.

A certain portion of the electrolytic decomposition products at 4 and 6 V is not soluble in acetonitrile, contains active carbon particles, attracts water, and the taste of acetic acid is perceptible, when it is dried at air. By help of GC-FID, we detected 0.2% to 0.6% of *acetic acid* in the acidified deposits on the active carbon anode. Free linear carboxylic acids higher than acetic acid play no role. In the cathodic residues, organic acid could not be detected at all.

Aromatic hydrocarbons, carboxylic acids, and quinones cannot be found in thermally aged electrolyte samples. Obviously they are generated by the catalytic activity of the carbon electrodes.

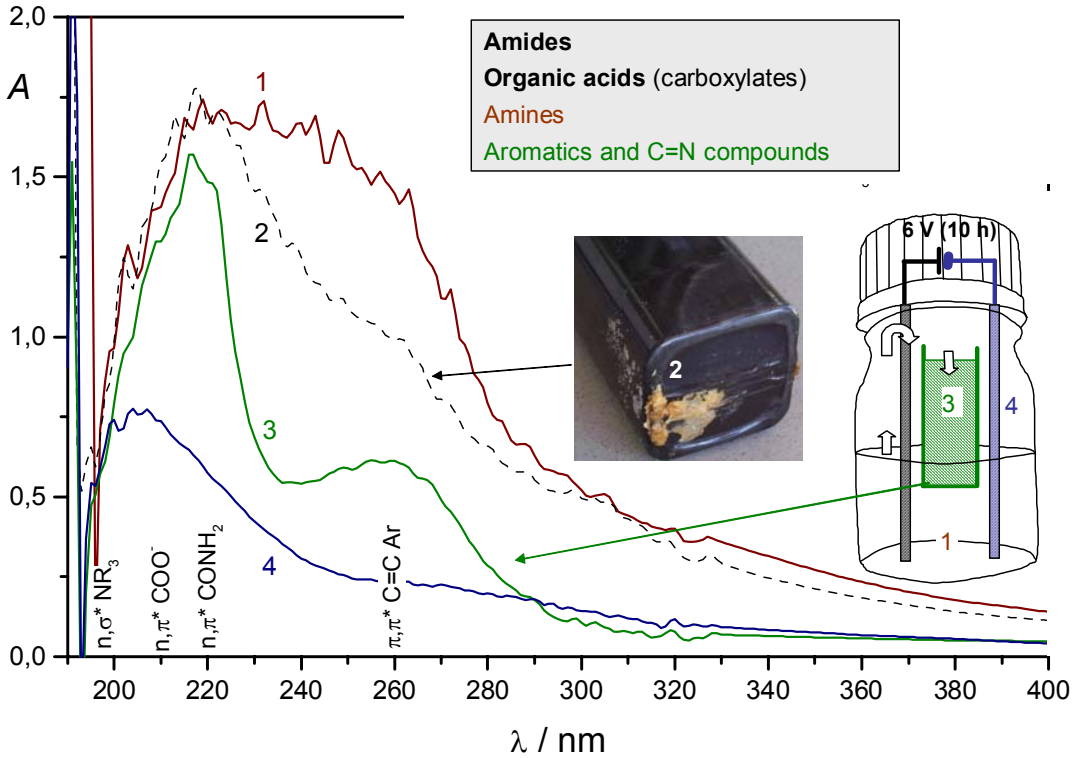

Fig. 5: UV/VIS spectrum of the residual electrolyte *1* (after electrolysis at 6 V, 10 h), absorbed gaseous products *3*, deposit on the cathode *4*, and crystals of the burst ultracapacitor *2*.

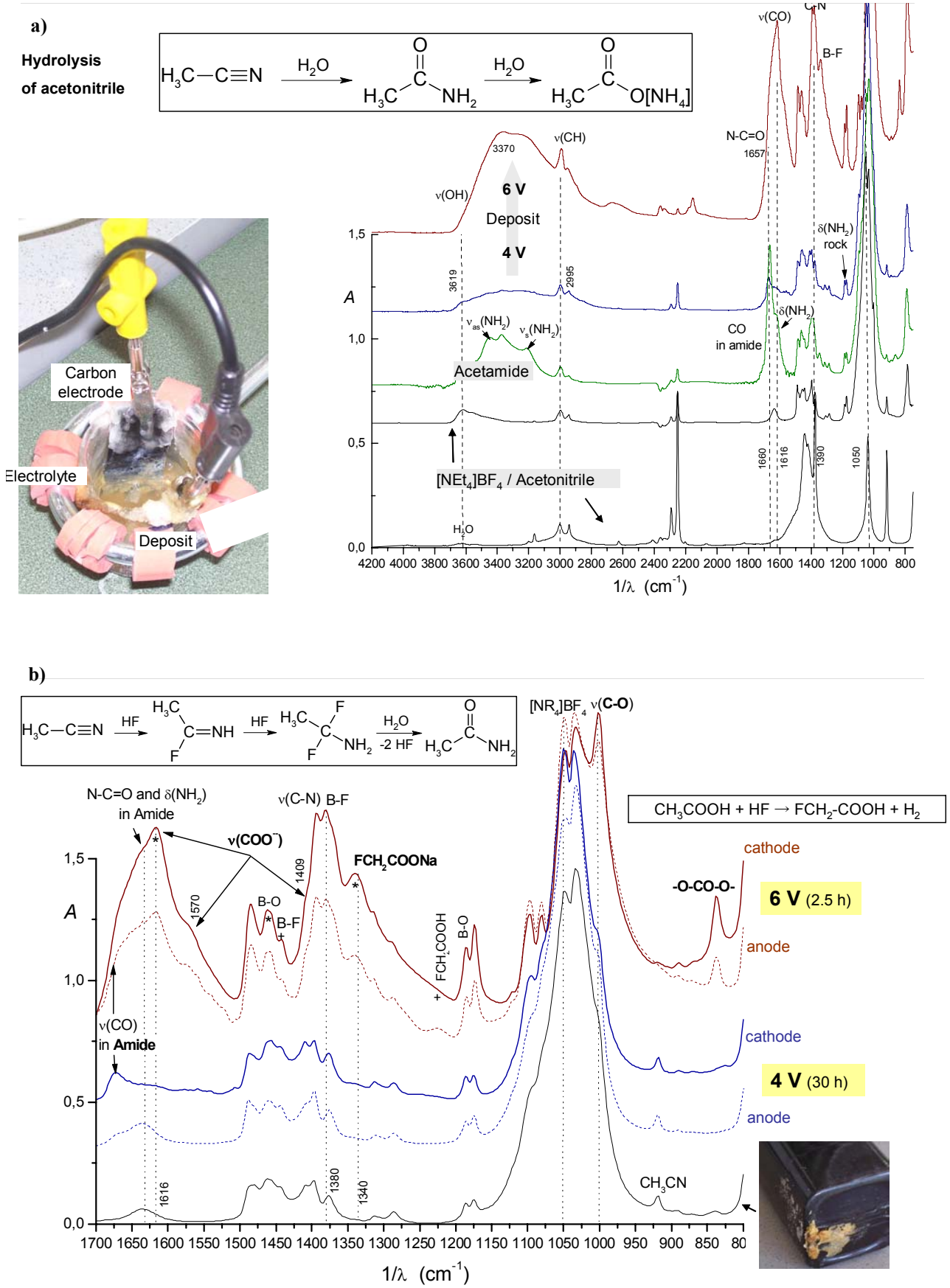

Fig. 6: a) FTIR spectra of the cathode deposit after electrolysis (*1* = 6 V, 2.5 h; *2* = 4 V, 30 h), in comparision to acetamide, fresh electrolyte and pure acetonitrile. – **b)** IR bands of amides and fluorocarboxylates in the electrolytic deposits and the crystals on the burst ultracapacitor.

1.5 Thermal decomposition products

Pure acetonitrile, and $TEABF_4$/acetonitrile electrolyte were aged in headspace vials for more than 500 hours at 70°C. We did not find any significant contaminations in the aged acetonitrile besides some butanenitrile. In the electrolyte sample, we detected negligible concentrations of fluorinated 2,3-butanediimine. Traces of *hydrogen fluoride* (mass 20) were present both in the pure and in the aged electrolyte.

As shown in **Figure 9**, in the liquid phase of acetonitrile and finished electrolyte, which were in contact to the electrode material, we found significant amounts of *alkyl substituted aromatics*, and cyclic siloxanes, which are dissolved from the electrode material already at room temperature. *Triethylamine* and *N*-alkyl-amines could be detected only in the electrolyte aged at 70 °C. Obviously the thermal decomposition of the $TEABF_4$ electrolye requires the catalytic activity of the electrode material. Pure acetonitrile behaves thermally stable.

1.6 Gaseous products in supercapacitors

In the headspace of the vials in Figure 8 we identified *ethylene* (mass 28), formed by splitting of the quarternary ammonium salt by a HOFFMANN elimination. The byproduct triethylamine and the tertiary amine radical $CH_3(C_2H_5)N{=}CH_2^+$ (mass 72) were found, too. As a result, a proton is set free which can form HF (mass 20) with excess fluoride.

In the gas space of real supercapacitors, which were aged uncharged at 70 °C for 500 hours, we found excess acetonitrile, water vapor, traces of oxygen, carbon dioxide and ethylene. In a volume of 100 µL, after chromatography at 120 °C at an unpolar column, the following masses were recorded.

Table 1: Fragement ions in the headspace of a commercial supercapacitor after aging at 70°C/500 h

Acetonitrile:	14 $CH_2^{+\cdot}$, 26 CN^+, 40/41 $CH_{2\text{-}3}CN^+$, less important: 15 CH_3^+, 27 HCN^+.
Gases:	18 H_2O^+, 28 $N_2^+/C_2H_4^+$, 32 O_2^+, 40 Ar, 44 CO_2^+ (besides $C_2H_6N^+$ from amine, $CONH_2^+$ from amides)
Fragments of the salt:	16 NH_2^+, 17 NH_3^+, 19 F^+; traces of 20 HF^+, 29 $C_2H_5^+$, 30 $BF^+/CH_2NH_2^+$, 39 $K^+/C_3H_3^+$, 43 $(CH_2)_2NH^+/CONH^+$, interestingly: 96 CF_3CONH fragment.

Mass 44 plays no role in the pure electrolyte, and is thus an indicator for the presence of triethylamine, already found in the liquid phase. The difference 44 $C_2H_6N^+ \rightarrow 16\ NH_2^+$ corresponds to the elimination of $CH_2{=}CH_2$ due to the onium reaction of *N*-ethylamines. The *fluoroacetamide* fragment (mass 96) supports our IR study for the model reactor.

In the headspace of a supercapacitor which was continously charged at 2.5 V and 70 °C, mass 44 and fluoride (mass 19) could be detected in significant larger amount, whereas mass 43 (from salt) dropped. Obviously, CO_2 is formed by the oxidation of carbon and the decarboxylation of organic acids.

We identified the fragments of *metaboric acid* and alkyl boron compounds – obviously generated by hydrolysis of BF_4-anions. As proof, IR bands of B-O vibrations in *inorganic borates* appear at 1460. 1054 and 780 cm^{-1} (see Figure 5).

1.7 The role of water

Commercial electrolytes contain less than 10 ppm of water. Absorbed water at carbon electrodes cannot completeley be removed even by drying at temperatures above 150 °C, because the organic binder between carbon particles and aluminium support is destroyed. The question is whether hydrogen gas, which is formed by electrolysis of water traces or the fluorination of carboxylic acids (SIMONS' process), is able to cause a drastical increase of pressure in the capacitor.

The electrolytical generaton of 1 ml hydrogen requires the electric charge of 8,6 C (2,4 mAh) and the volume of 0,8 ml water. 10 ppm water equal about 8,5 ml in one liter of electrolyte solution. Hence, 100 ml of electrolyte, containing 0,85 mg water, are enough to produce about 1 ml hydrogen gas (1 mg H_2O = 1,245 ml H_2) to expand the case.

1.8 Corrosion products at the electrodes

The carbon/aluminium electrodes were investigated by TOF-SIMS after the aging experiment in headspace vials at 70 °C for 550 hours. White spots appeared on the part of the aluminium foil which was immersed in the electrolyte. The mass spectrum in **Figure 10** shows deposits of $[(C_2H_5)_4N]BF_4$ and a mixture of hydrocarbons with long chains (mass 300 to 700). Besides the expected Al^+ signal, fluoroaluminate and fluorooxy aluminate complexes of the kind AlF_4^-, $AlF_4[AlOF]_n^-$, $AlF_4AlF_3(AlOF)_n^-$, and $AlF_2O(AlOF)_n^-$ are present. The white spots on the part of the electrodes, which was in contact to air, show the highest intensities of the Al/F/O clusters. Signals of the kind $[Al_2O_3]_nOH^-$, which are usually found on oxydized aluminium surfaces, are completely missing.

Obviously the aluminium support under the carbon layer is attacked by *aggressive fluoride*. It is known from literature that aluminium fluorides are more stable than fluoroboron compounds. Hence, we consider the dissolving Al_2O_3 layer on the etched aluminium support below the active carbon layer as a possible source of oxygen for the borate formation.

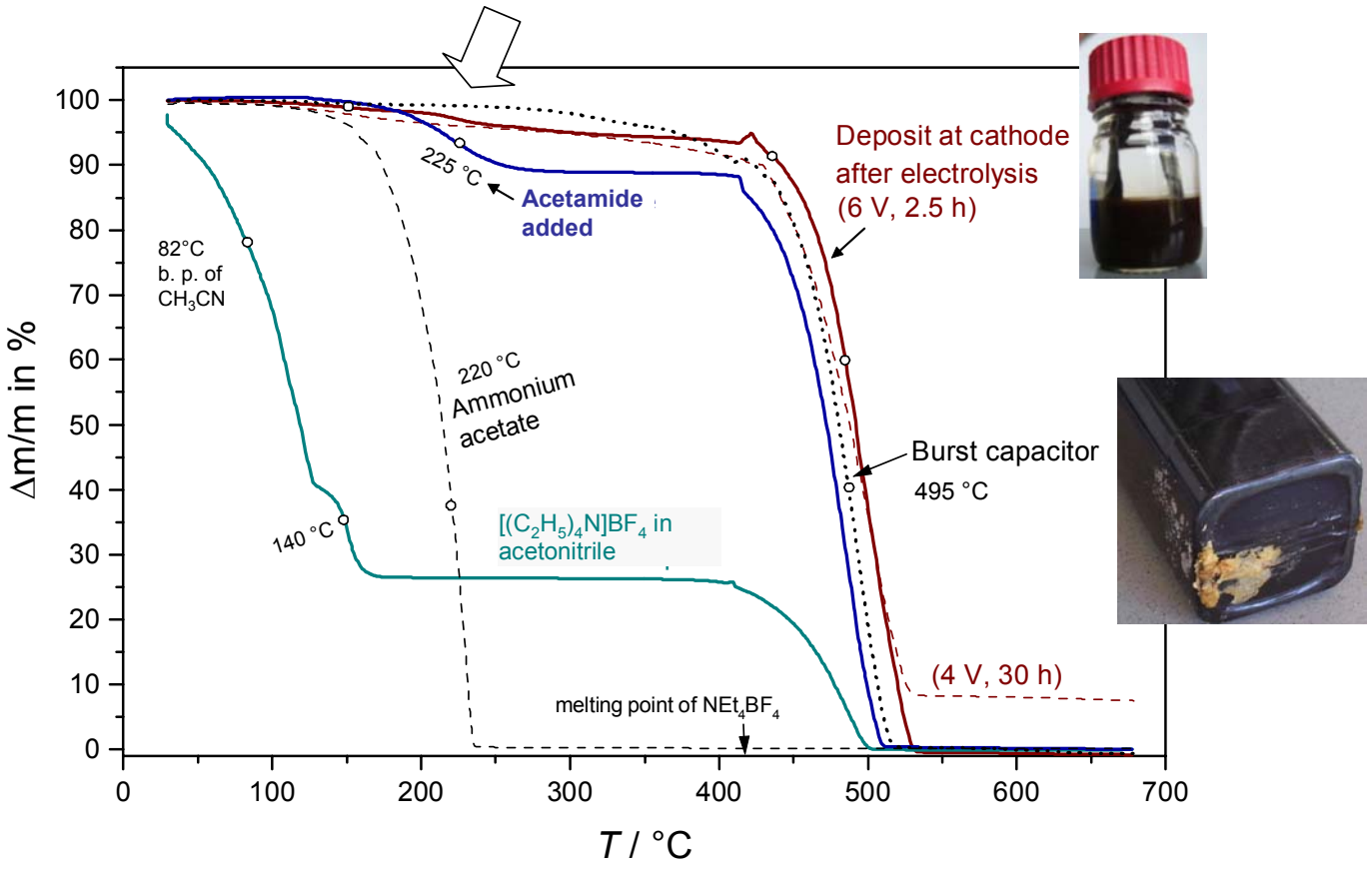

Fig. 7: Thermogravimetric analysis (TGA) of the electrolytic deposits (see Figure 4) in comparison with the bloom on the burst ultracapacitor (dashed line).

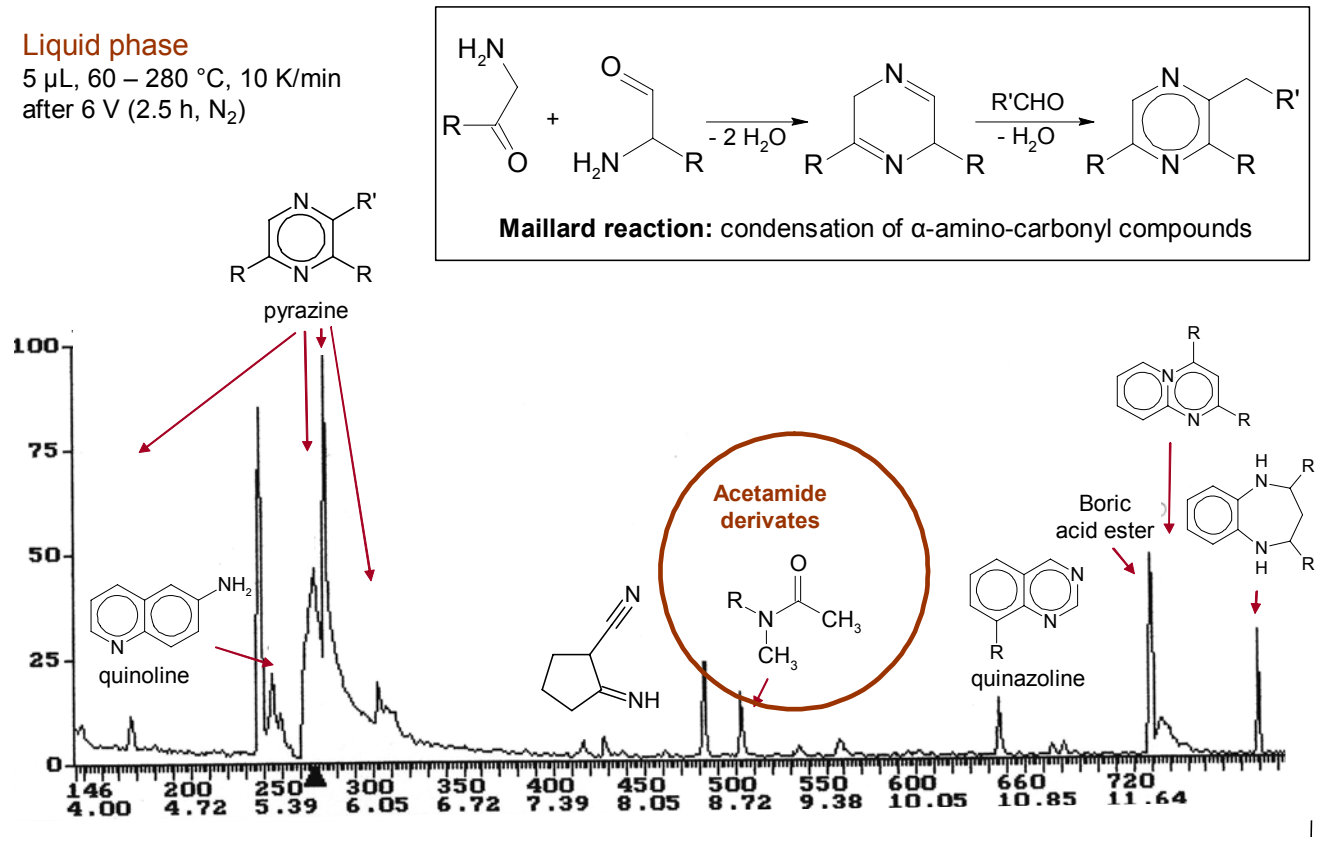

Fig. 8: GC-MS analysis (70 to 280 °C at 10 °C/min) of the electrolysis products in the liquid $[(C_2H_5)_4N]BF_4$/acetonitrile phase (6 V, 2.5 h, N_2, see Figure 4).

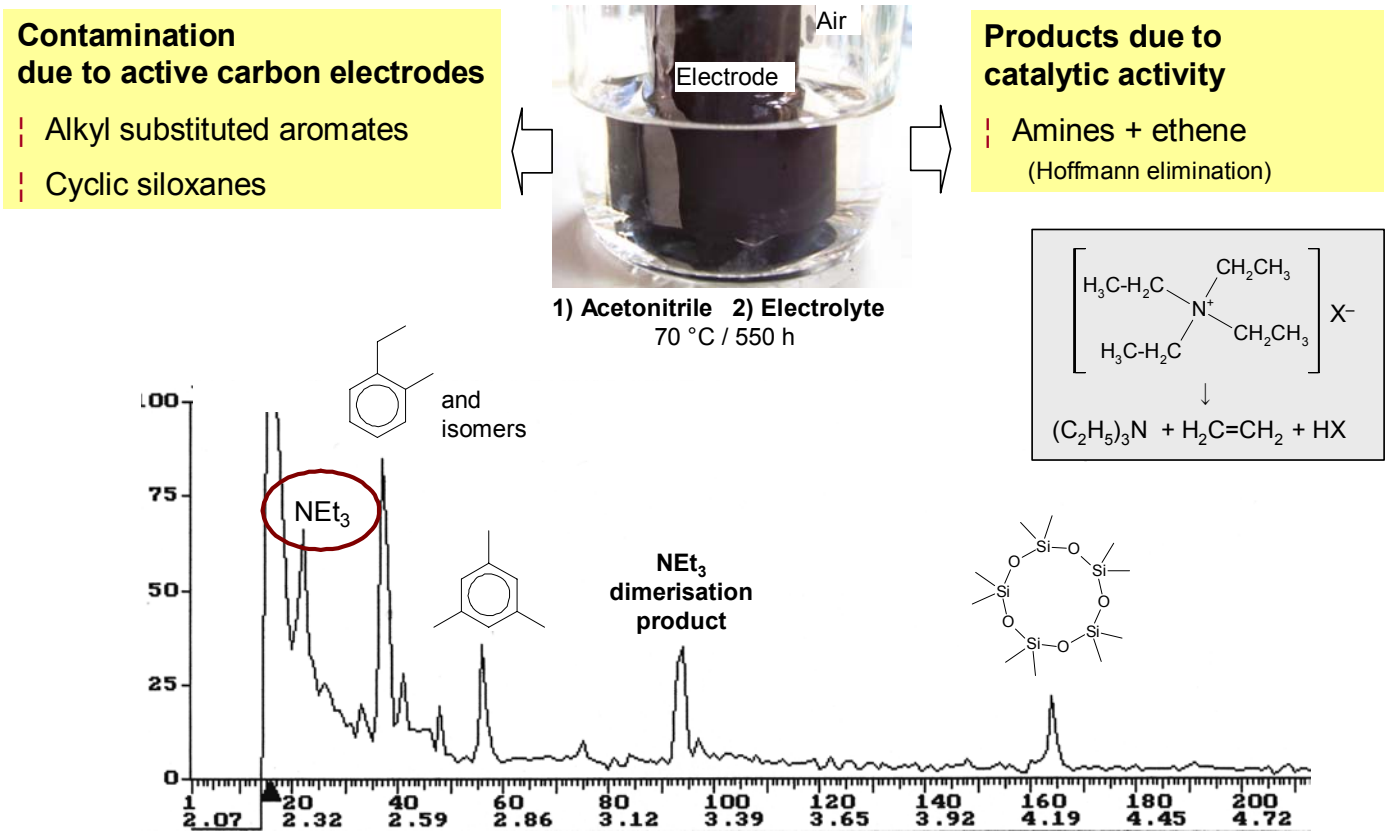

Fig. 9: GC-MS analysis of the thermal decomposition of $TEABF_4$/acetonitrile in presence of an active carbon electrode (70 °C, 550 hours).

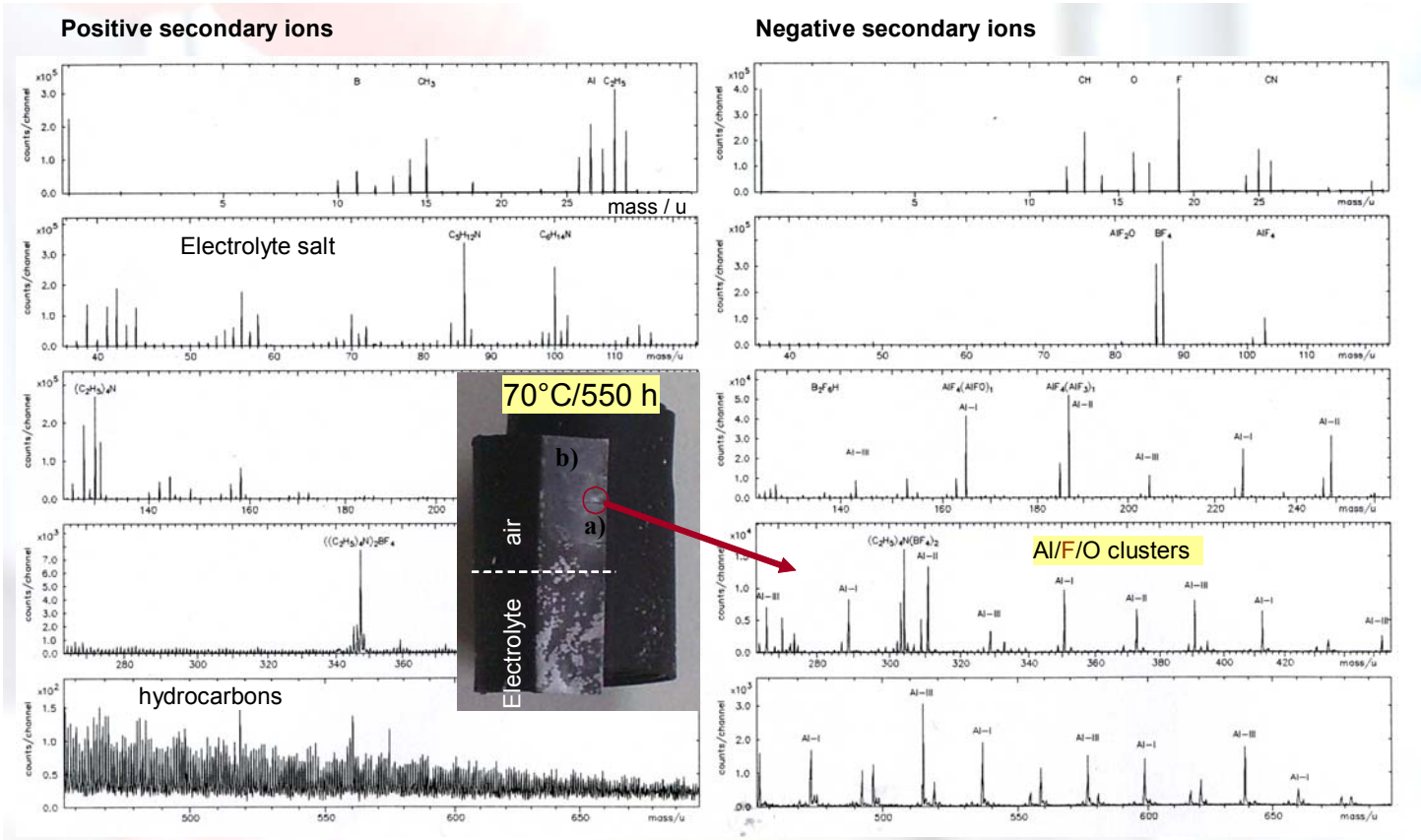

Fig. 10: a) TOF-SIMS spectrum of the white spots on the aluminium support below the active carbon layer after aging in $(C_2H_5)_4NBF_4$/acetonitrile. – b) Pure aluminium support: tenfold lower intensities of the Al/F/O clusters.

2 Ionic liquids and nanomaterials

2.1 Frequency response of ionic liquids

Electrolytes based on acetonitrile and propylene carbonate are limited to a potential window of about 2.7 V, but their conductivity of about 100 mS/cm comes close to inorganic electrolytes such as sulfuric acid (850 mS/cm) and potassium hydroxide (620 mS/cm).

a) We investigated different ionic liquids [6] with respect to their use in supercapacitors by *ac* impedance spectroscopy in a frequeny range between 10 kHz to 0.1 Hz. The measuring cell, shown in **Figure 11,** comprised two gilt copper stamps in a fixed distance of 2 mm. The vacuum capacitance of $C_0 \approx 3$ pF at 1 kHz was verified by a LCR bridge. The cell constant $K = R \cdot \kappa \approx 0.027$ cm^{-1} was determined by help of 0.1 molar KCl solution (κ = 0.01215 S/cm, 22°C) and the measured impedance real part R at 1 kHz. Capacitance at any circular frequency f was calculated from the imaginary part of impedance with reference to a simple R–C series combination.

$$C = \varepsilon K = \frac{-1}{2\pi f \cdot \mathrm{Im}\underline{Z}(\omega)} \qquad (2.1)$$

Figure 11 exhibits the low resistance and high capacitance of $[(C_2H_5)_4N]BF_4$ in acetonitrile in comparison to novel ionic liquids.

b) The temperature dependence of conductivity and permittivity – shown in **Figure 13** – was investigated by help of an temperature controlled glass vessel filled with 25 ml of ionic liquid, a glassy carbon working electrode, and a platinum counter electrode. The cell constants K were 0.742 (25°C), 0.790 (40°C), 0.850 (60°C), 0.905 (70°C), 1.204 (85°C), based on literature values for the conductivity of a 1-molar potassium chloride solution,

$$\kappa(T) = 0{,}00193\ T/°\mathrm{C} + 0{,}0634 \text{ (in S/cm)},$$

at a frequency of 10 kHz. Conductivity, calculated by help of the real parts of impedance according to $\kappa(\omega) = K/R(\omega)$, increases with temperature, which was to be expected for ionic conductors. Arrhenius plots were constructed by help of the resistance values at 1 kHz.

The quantity $\varepsilon = 70 \cdot C$ / 0.77 mF was calculated as a rough estimate of dissociation and interionic forces. The measured capacitance C was divided by the capacitance of 1-molar KCl solution at 0.5 Hz and multiplied by its permittivity of 70 at 25°C [7], which slightly decreases at higher temperatures.

Summarizing, organic electrolytes based on acetonitrile show the best conductivity of all solvent systems we have known so far. AMMOENG, a commercial product, excels at an enjoyably small frequency-dependence of capacitance, but its resistance is 200 times higher compared with $TEABF_4$/acetonitrile.

2.2 Voltage window

Wide voltage windows reported in literature [6] refer to highly cleaned and dried samples of ionic liquids. The voltammograms in **Figure 12** show acetonitrile/ $TEABF_4$ as the most stable solution. Traces of air and moisture were allowed with respect to the technical applications and aging. Thus, supercapacitor cells built of commercial active carbon electrodes and ionic liquids, absorbed by polymer separators, did not reveal any advantage compared to $(C_2H_5)_4NBF_4$/acetonitrile.

The decomposition voltage of $[BMIM]BF_4$ equals about 2.5 V at anodic potentials, and about –4 V at cathodic potentials. Unfortunately, ionic liquids tend to *decompose and polymerize* after several hundred charge/discharge cyles. The ionic liquids in the test showed an unwanted leakage current due to decomposition reactions already at cell voltages around 1.5 to 2 V, especially $[BMIM]OcSO_4$, AMMOENG^{TM}102, and $[MMIM]Me_2PO_4$. The formation of gas bubbles, white polymer-like strings, and a brownish tinge were observed.

2.3 Carbon nanomaterials

Active carbon electrodes bound on aluminium foils have been the most successful commercial materials so far.

Figure 14 shows the *ac* impedance spectra (capacitance versus resistance) of aluminium foils which were coated with nanomaterials in a thin and a thick layer. The thicker the active layer is, the more increases the resistance of the supercapacitor cell. However, *nanofibres* show an advantage in *dc* capacitance in contrast to active carbon.

Due to the lower contact resistance between active material and aluminium foil, the commercial electrode (as shown in Figure 2) exhibits the best frequency response at the left upper side at low resistance and high capacitance [8].

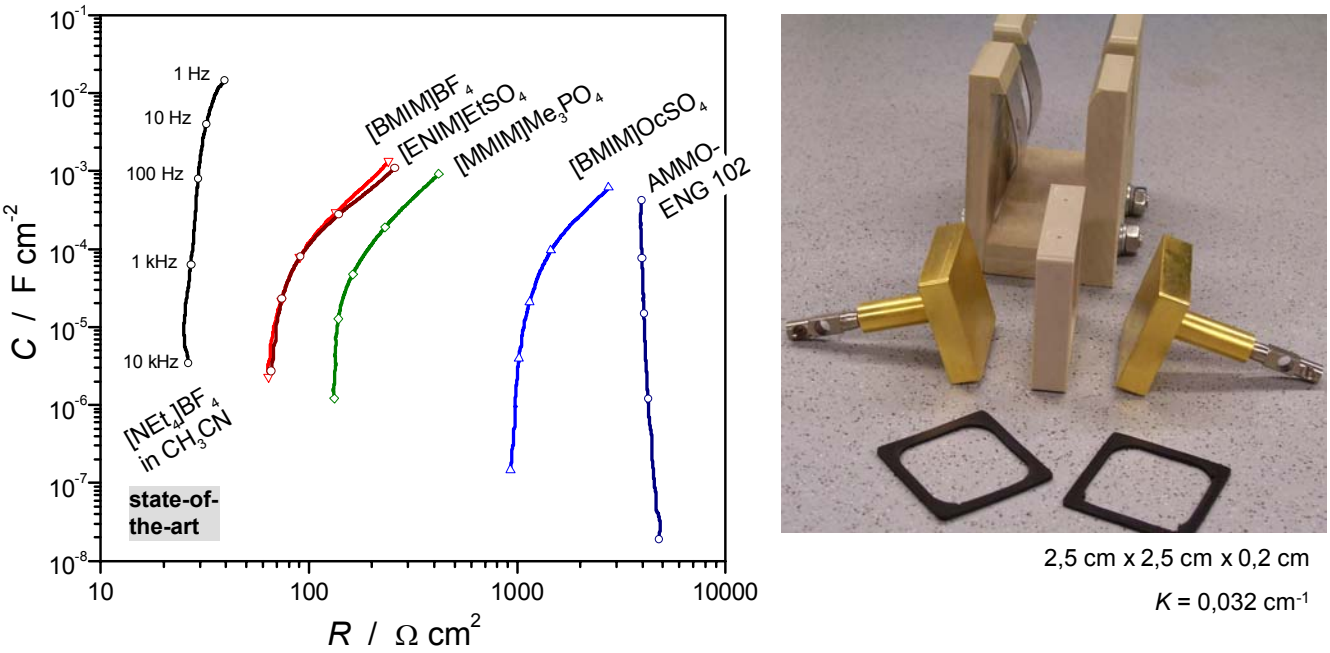

Fig. 11.: *Left:* Frequency response of capacitance and resistance of different ionic liquids in camparsion with $TEABF_4$/acetonitrile at room temperature (22°C). – *Right:* Cell of two gilt copper stamps, polymer spacer and seals.

$[BMIM][OcSO_4]$	= 1-Butyl-3-methyl-imidazolium octylsulfate
$[BMIM][BF_4]$	= 1-Butyl-3-methyl-Imidazolium tetrafluoroborate
$[MMIM][Me_2PO_4]$	= 1,3-Dimethyl-imidazolium dimethylphosphate
$[EMIM][EtSO_4]$	= 1-Ethyl-3-methyl-imidazolium ethylsulfate
AMMOENG	= commercial ionic fluid by "Solvent Innovation", Cologne, Germany

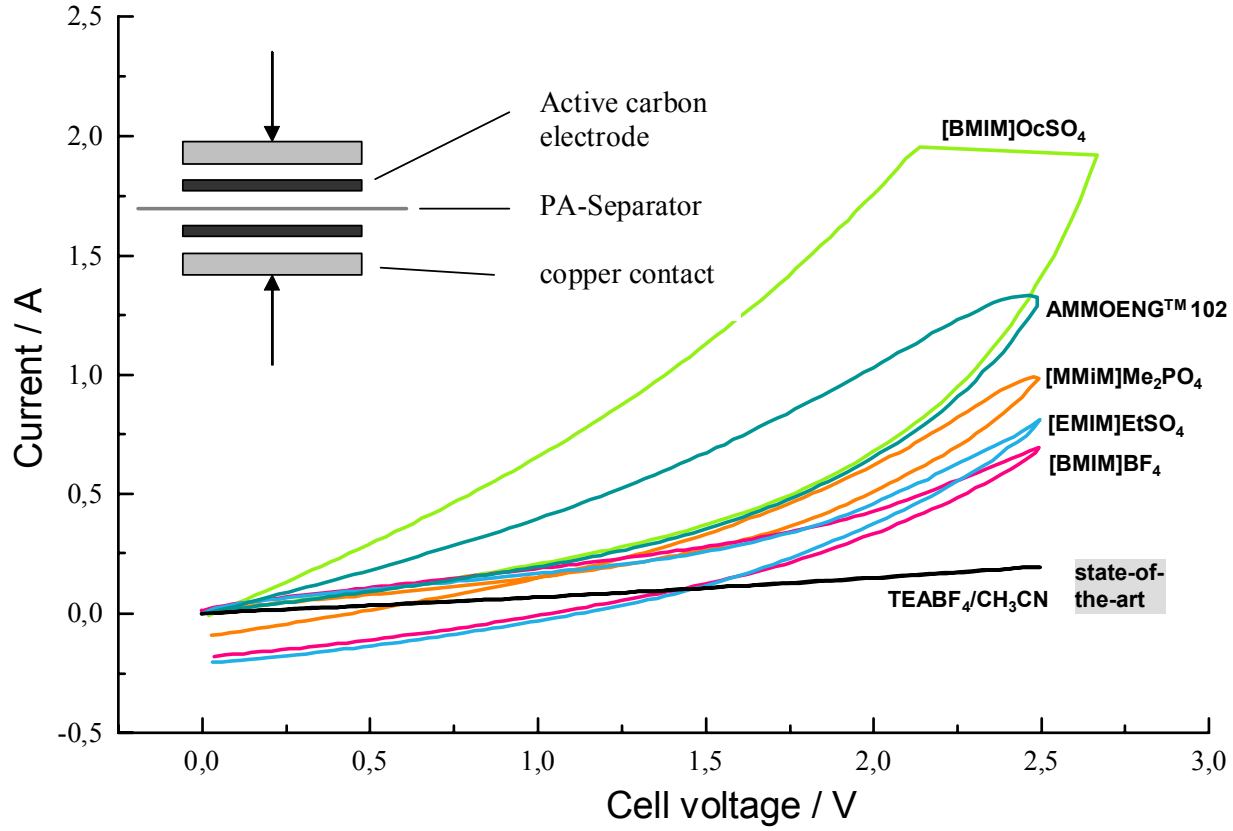

Fig. 12: Cyclic voltammograms of ionic liquids (without preceding cleaning processes) in capacitor cells at 22°C.

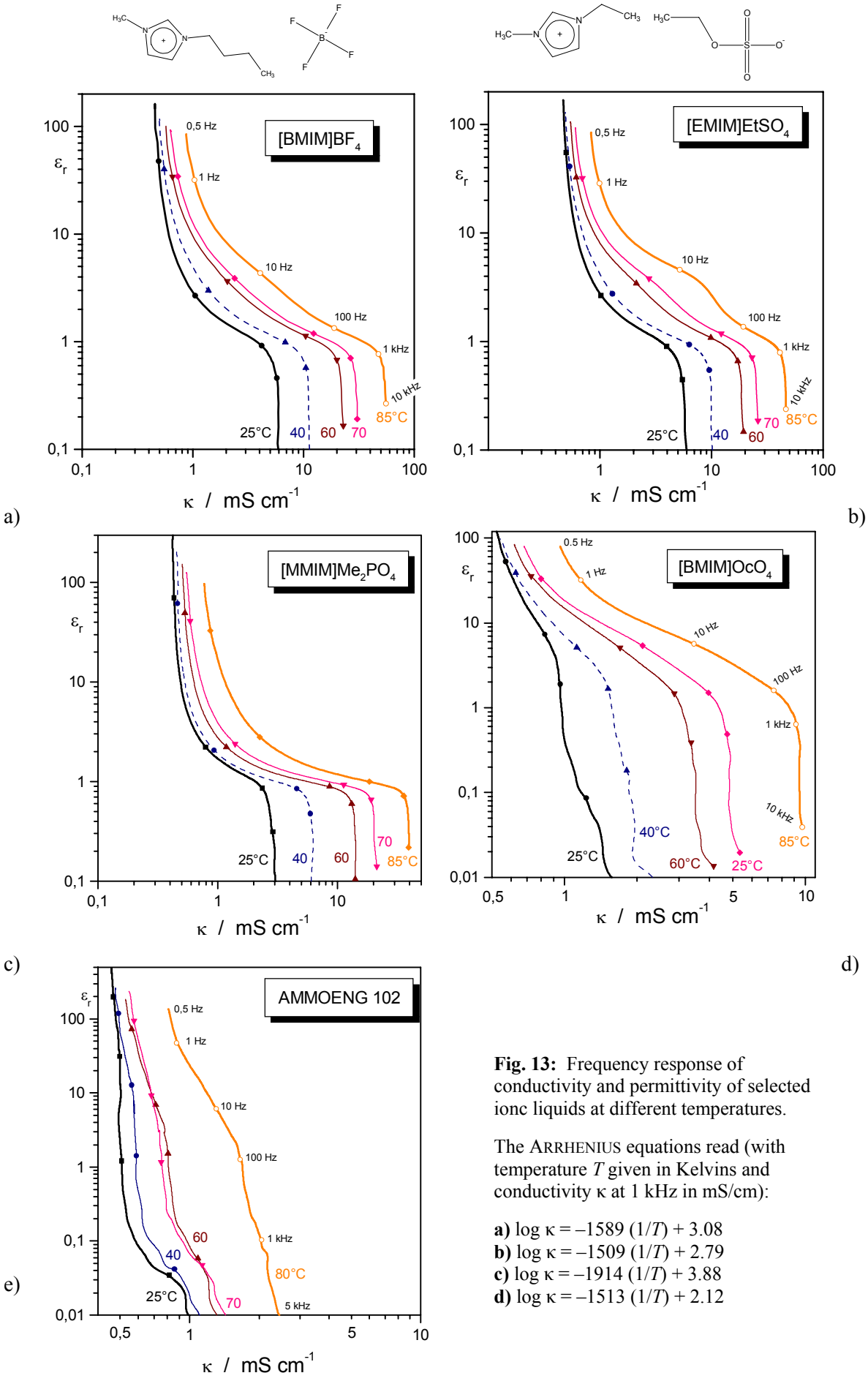

Fig. 13: Frequency response of conductivity and permittivity of selected ionc liquids at different temperatures.

The ARRHENIUS equations read (with temperature T given in Kelvins and conductivity κ at 1 kHz in mS/cm):

a) $\log \kappa = -1589\ (1/T) + 3.08$
b) $\log \kappa = -1509\ (1/T) + 2.79$
c) $\log \kappa = -1914\ (1/T) + 3.88$
d) $\log \kappa = -1513\ (1/T) + 2.12$

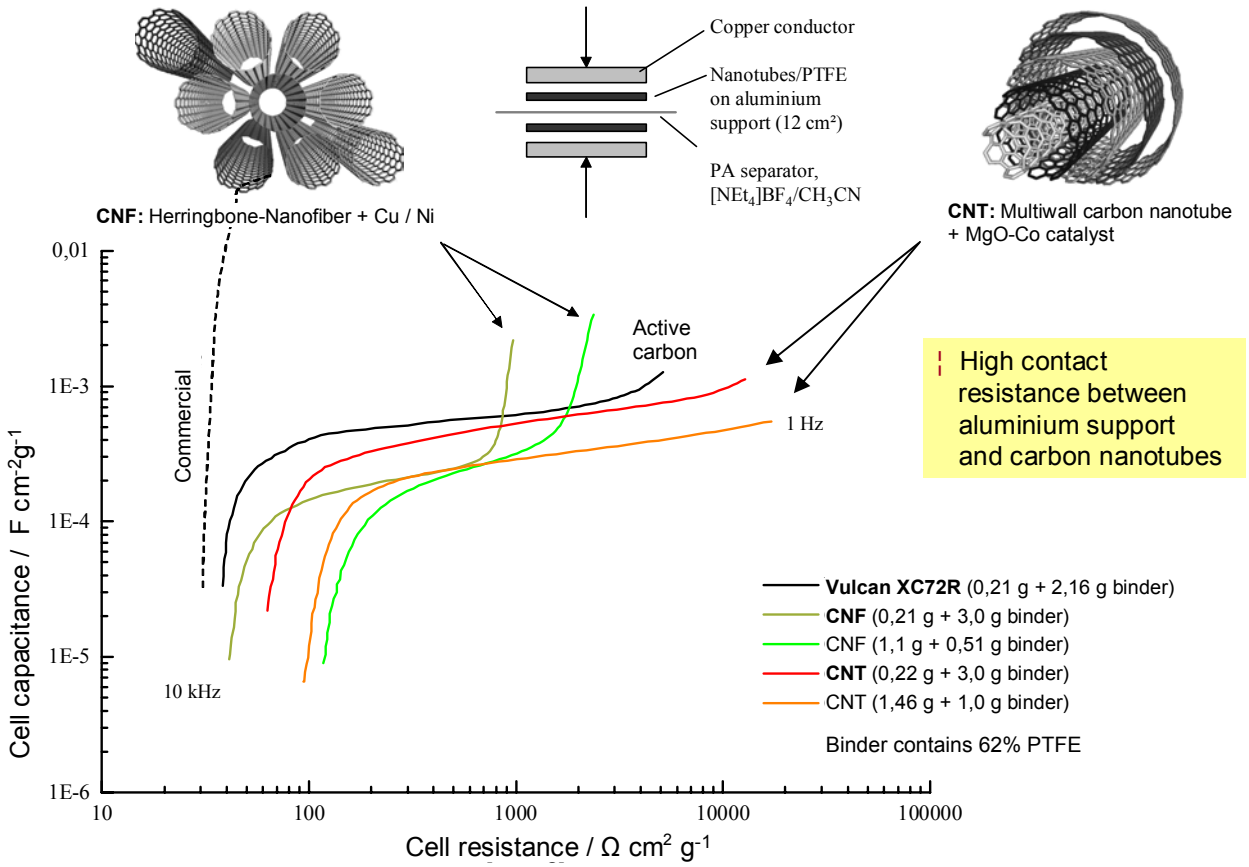

Fig. 14: Frequency response of specific capacitance (per unit area and gram of active mass) and resistance of supercapacitor cells: nanomaterials coated on aluminium foil in comparision to active carbon "Vulcan" – and commercial active carbon electrodes (see Fig. 2) . Temperature 22°C.

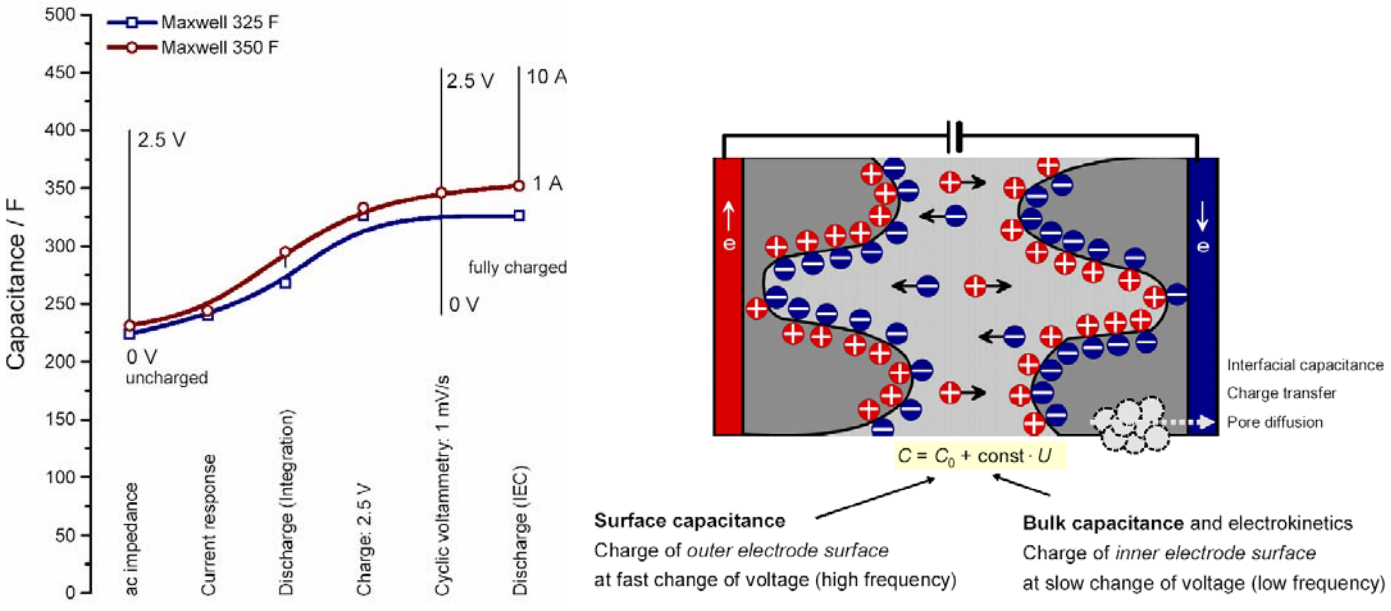

Fig. 15: Capacitance of a MAXWELL 350 F supercapacitor (BCAP0350) determined by fast and slow techniques working in different voltage ranges and states-of-charge of the supercapacitor.

3 Determination of rated capacitance

3.1 Capacitance measurement in practice

Industrial quality assurance during the fabrication of supercapacitors requires reliable and time-saving methods to determine rated capacitances. As we stressed in the last year seminar [1], capacitance is a function of voltage and the state-of-charge of the supercapacitor, respectively.

- Capacitance determined by electrochemical techniques working in different time domains yield basically different values of capacitance. **Figure 15** illustrates that *ac* impedance spectroscopy, chronoamperometry, and constant current discharge reflect different capacitive processes at the outer surface (if the excitation signal is fast) and the inner surface (at *dc* measurements) of the porous electrode/electrolyte interface.
- Capacitance appears as a dynamic quantity that can be divided up in a double-layer capacitance at the "outer" electrode surface and a pseudo-capacitance due to slow faradaic processes depending on voltage: $C = C_0 + kU$, whereby C_0 is the capacitance at 0 V. Transient techniques, which generate fast voltage changes, reflect the fast charge/discharge processes with "frozen" diffusion at the outer electrode surface. At slow voltage alteration the reactions controlled by diffusion in the inner electrode surface (strongly depending on voltage) contribute to the measured capacitance values.
- Constant current discharge according to IEC 40/1378 [8] yields the highest capacitance values. By this method, the linear drop of the rated voltage from 80% to 40% is evaluated (see Figure 15).

Figure 16 shows that the IEC-value is a more or less good approximation of average differential capacitance in the constant current discharge test. *Differential capacitance* was calculated by help of the inifinitesimal voltage drop at each point in time.

$$C(t) = \frac{I(t)}{\mathrm{d}U(t)/\mathrm{d}t} \tag{3.1}$$

Due to the measurement error of the voltage values $\Delta U(t) \approx 10\ \mu V$, and the small time intervals of less than 1 ms, the derivative $\mathrm{d}U/\mathrm{d}t$ was smoothed by an FFT algorithm.

Integral capacitance calculated according to equation 3.2 shows a bit lower values.

$$C(t) = \frac{Q(t)}{U_0 - U(t)} = \frac{1}{U_0 - U(t)} \int_0^t I(t')\,\mathrm{d}t' \tag{3.2}$$

Electric charge Q was determined by help of the trapezoidal rule at each point in time. In the special case that the average value of discharge current is considered as constant, the simple IEC-method can be derived if equation 3.4 is reduced to 2 points.

$$Q(t_n) = \frac{1}{2}\sum_{i=1}^{n}(I_i + I_{i-1})(t_i - t_{i-1}) = \bar{I} \cdot t_n \tag{3.3}$$

$$C = \frac{Q_i - Q_{i-1}}{U_i - U_{i-1}} = \frac{I \cdot (t_i - t_{i-1})}{U_i - U_{i-1}} \tag{3.4}$$

The IEC method provides a capacitance value (46.8 F) that is higher than the average value of differential capacitance in the full voltage window of discharge (45.6 F). This result affirms Figure 15.

3.2 Scaling factors for *ac* impedance spectroscopy

Figure 17 shows that *ac* impedance spectroscopy [9] at frequencies below 0.1 Hz is able to provide rated capacitance of supercapacitors. Interestingly, the capacitance values printed on the capacitor cases cannot be confirmed for every manufacturer.

Fast *ac* impedance measurements allow to gather series resistance at 100 Hz and capacitance at 1 Hz within about 30 seconds. Rated *dc* capacitance must be extrapolated by multiplying the 1 Hz capacitance with a scaling factor *f* according to **Table 2**.

$$C_{\mathrm{dc}} = f \cdot C_{1\mathrm{Hz}} = \begin{cases} 1.5 \cdot C_{1\mathrm{Hz}} & \text{(acetonitrile)} \\ 5 \cdot C_{1\mathrm{Hz}} & \text{(propylene carbonate)} \end{cases} \tag{3.5}$$

The scaling factor depends primarily on the electrode/electrolyte system. Size and geometry of the capacitor play a secondary role. The scaling factor is obtained by dividing the average value of *dc* capacitance by the average value of *ac* capacitance at 1 Hz.

Table 2: Rated capacitance (in F) and series resistance determined for a lot of supercacitors. The given error equals the experimental standard deviation.

	Aceonitrile		Propylencarbonate	
Rated value	50 F	100 F	50 F	100 F
Cyclic voltammetry				
at 0.02 V/s	51 ± 1.7	112 ± 1.8	41 ± 0.7	80 ± 0.8
***ac*-impedance spectroscopy**				
at 0.01 Hz at 1 Hz	50 33.7 ± 2.3	110 65.0 ± 8.2	34 7.14 ± 0.56	66 14.7 ± 0.54
Scaling factor $C_{0.01\mathrm{Hz}}/C_{1\mathrm{Hz}}$ $C_{\mathrm{CV}}/C_{1\mathrm{Hz}}$	 1.5 1.5	 1.7 1.7	 4.8 5.7	 4.5 5.4
Resistance at 100 Hz	14.8 ± 1.2 mΩ	13.0 ± 2.2 mΩ	31.2 ± 2.0 mΩ	22.2 ± 6.5 mΩ

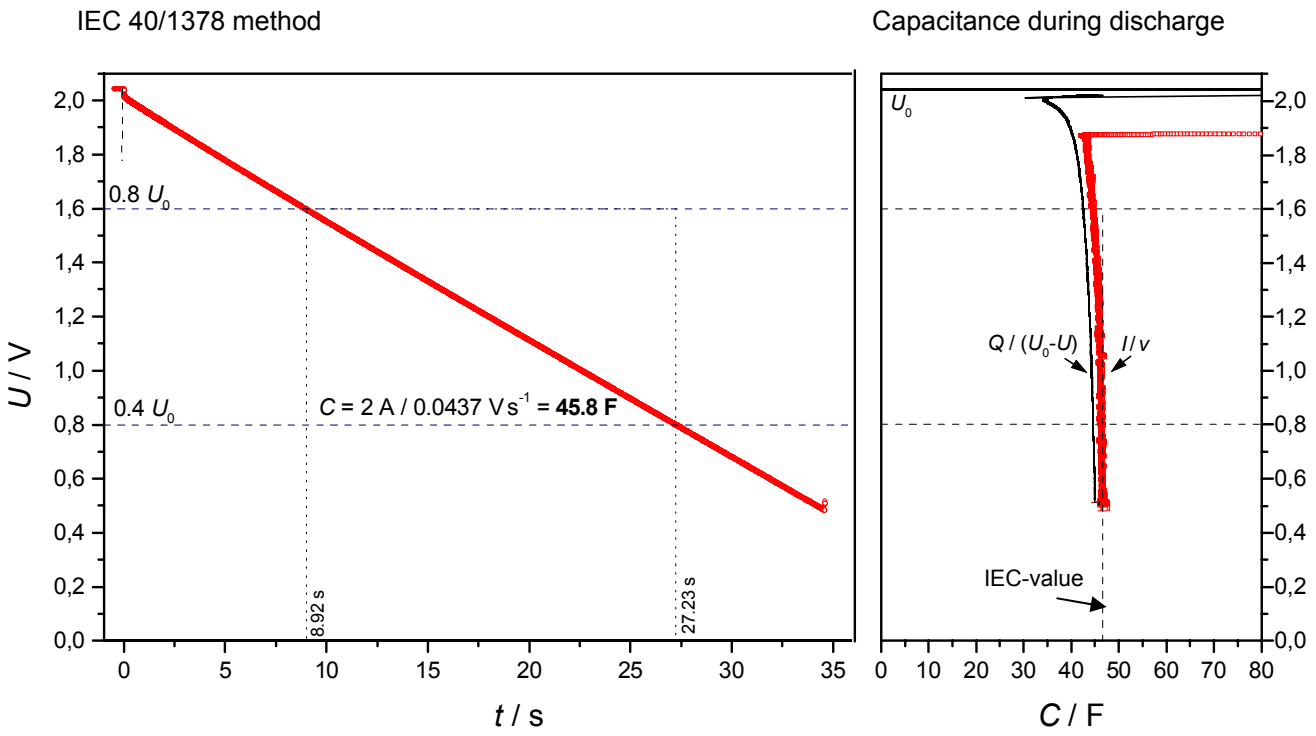

Fig. 16: Capacitance of a 50 F supercapacitor, charged at 2.0 V, determined by the IEC method at a discharge current of 2 A (*left*) and "true" differential capacitance *(right*, see text).

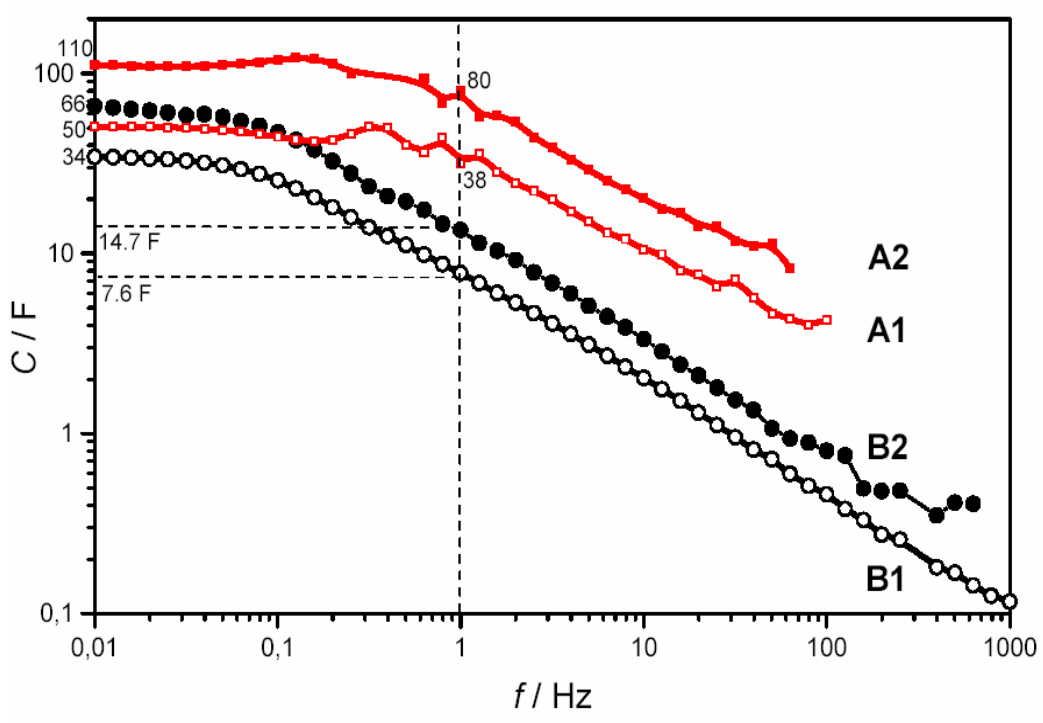

Fig. 17: Frequency response of capacitance $C = -[2\pi f \cdot \mathrm{Im}\ Z]^{-1}$ of supercapacitors with different electrolyte systems (**A:** acetonitrile, **B:** propylencarbonate) rated at **1** = 50 F, and **2** = 100 F by the manufacturers.

3.3 Reliable *dc* capacitance by CV

Cyclic voltammetry [1] at low scan rates proved as a most precise, robust and uncorrupible method to determine rated capacitance. Charge and discharge cycle were averaged in the usable voltage window ΔU between 0 and 2.7 V to yield the values in **Table 2.**

$$C = \frac{Q_{\text{in}} + Q_{\text{ex}}}{2 \cdot \Delta U} = \frac{1}{2v \cdot \Delta U}\left[\int_0^{\Delta U} I_{\text{in}}(U)\,\mathrm{d}U + \int_{\Delta U}^{0} I_{\text{ex}}(U)\,\mathrm{d}U\right]$$

$$\text{and} \quad v = \frac{\mathrm{d}U}{\mathrm{d}t} = 0.02 \text{ V/s} \qquad (3.6)$$

3.4 A novel quality criterion

In order to simplify industrial quality control by fast *ac* impedance spectroscopy, we propose the following dimensionless quantity.

$$g = \frac{C_1}{R_{100}} \cdot \frac{R_{\text{n}}}{C_{\text{n}}} >> 1 \qquad (3.7)$$

C_1 measured series *ac* capacitance at 1 Hz
R_{100} measured series resistance at 100 Hz
R_{n} rated resistance, average of the R_{100}-values of all capacitors in the test
C_{n} rated capacitance, e. g. average value measured by slow cyclic voltammetry

The quantity g gets a big value for capacitors with high capacitance and slow resistance. The example in **Figure 18** shows four lots of supercapacitors.

The horizontal line $g = 1$ marks "average quality". The best capacitors lie clearly above 1, and the worst samples lie below 1. The A2 type capacitors really provide the highest capacitance and the lowest resistance useful for the technical application, although the B2 type was designated with the identical rated values by a different manufacturer.

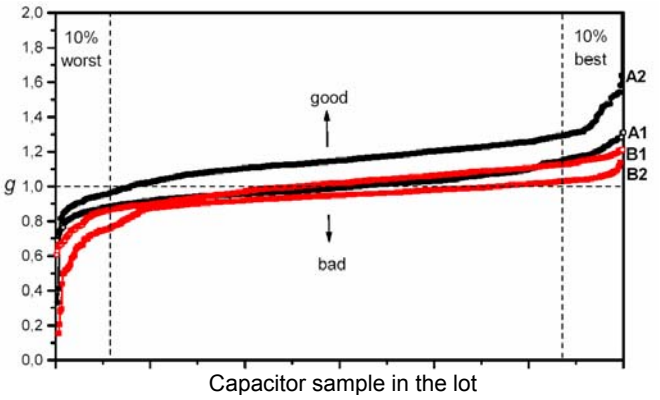

Fig. 18: Quality quantity g for good and bad lots of supercapacitors of different lots (A and B), rated at 1 = 50 F, and 2 = 100 F.

Acknowledgement – The authors wish to thank our student A. ROTHÄUGER for valuable measurements.

4 References

[1] P. KURZWEIL, B. FRENZEL, R. GALLAY, Capacitance Characterization Methods and Ageing Behaviour of Supercapacitors *Proc. 15th International Seminar On Double Layer Capacitors,* Deerfield Beach, U.S.A., December 5-7, 2005.

[2] P. KURZWEIL, M. CHWISTEK, Electrochemical Stability Of Organic Electrolytes In Supercapacitors: Spectroscopy And Gas Analysis Of Decomposition Products, *Proc. 10th Ulm Electrochemical Talks* (UECT), June 27-28, 2006; to be published in *J. Power Sources*.

[3] P. KURZWEIL, M. CHWISTEK, R. GALLAY, Electrochemical and Spectroscopic Studies on Rated Capacitance and Aging Mechanisms of Supercapacitors Based on Acetonitrile, *Proc. 2nd European Symposium on Super Capacitors & Applications* (ESSCAP), Lausanne, 2006.

[4] Literature listed by www.scirus.com.

[5] Spectral data in digital databases.

[6] P. C. TRULOVE, R. A. MANTZ, Electrochemical properties of ionic liquids, in: P. WASSERSCHEID, T. WELTON (Eds.), *Ionic Liquids in Synthesis*, Wiley-VCH, Weinheim

[7] G. KORTÜM, *Lehrbuch der Elektrochemie*, Verlag Chemie, Weinheim 1970, p. 140.

[8] IEC-40/1378 / DIN IEC 62391-1, Fixed electric double layer capacitors for use in electronic equipment. Part I: Generic specification, June 2004. IEC-40/1379 / DIN IEC 62391-2, Fixed electric double layer capacitors for use in electronic equipment. Part I: Sectional specification: Electric double layer capacitors for power application, June 2004.

[9] P. KURZWEIL, H.-J. FISCHLE, A new monitoring method for electrochemical aggregates by impedance spectroscopy, *J. Power Sources* **127** (2004) 331–340.